CONF-801072--11

THE STRUCTURE AND COMPOSITION OF PHASES OCCURRING IN AUSTENITIC STAINLESS STEELS IN THERMAL AND IRRADIATION ENVIRONMENTS*

E. H. Lee, P. J. Maziasz, and A. F. Rowcliffe
Metals and Ceramics Division
Oak Ridge National Laboratory

Transmission electron diffraction techniques coupled with quantitative x-ray energy dispersive spectroscopy have been used to characterize the phases which develop in austenitic stainless steels during exposure to thermal and to irradiation environments. In AISI 316 and Ti-modified stainless steels some thirteen phases have been identified and characterized in terms of their crystal structure and chemical composition. Irradiation does not produce any completely new phases. However, as a result of radiation-induced segregation principally of Ni and Si, and of enhanced diffusion rates, several major changes in phase relationships occur during irradiation. Firstly, phases characteristic of remote regions of the phase diagram appear unexpectedly and dissolve during postirradiation annealing (radiation-induced phases). Secondly, some phases develop with their compositions significantly altered by the incorporation of Ni or Si (radiation-modified phases). In addition, several phases develop at significantly lower temperatures during neutron irradiation (radiation-enhanced phases).

* Research sponsored by the Division of Reactor Research and Technology and Office of Fusion Energy, U.S. Department of Energy under contract W-7405-eng-26 with the Union Carbide Corporation.

Introduction

The need to develop structural alloys which will withstand high levels of displacement damage in breeder reactors and Magnetic Fusion Energy (MFE) machines has revitalized interest in the effects of radiation on solid state precipitation processes. It has recently been shown that both void swelling and irradiation creep behavior of complex alloys are strongly influenced by the sequences of precipitation reactions which occur during irradiation. The major theoretical and experimental efforts in this field have been directed towards understanding binary alloy systems. Several important radiation induced phenomena have been defined, e.g., a) enhanced diffusion, b) precipitate nucleation on point defect clusters or loops, c) segregation resulting from the coupling between solute and point defect fluxes , d) radiation induced ordering and disordering, e) stabilization and destabilization of phases by vacancy fluxes, f) cascade dissolution. These phenomena substantially modify the phase mixture which normally develops during thermal aging, e.g., a) the relative proportions of phases may be altered, b) the particle size distribution and number density may be different, d) phases characteristic of another region of the phase diagram may develop either as a result of segregation, or because of changes in the relative free energies of phases.

The austenitic stainless steels used for reactor applications such as AISI 316, are complex alloys, and typically up to eight major phases may develop during thermal aging in the temperature range of technological interest. In high temperature irradiation environments the relationships between these phases are altered and unexpected phases frequently develop. In the work described here, we have applied transmission electron microscopy (TEM), coupled with x-ray energy dispersive spectroscopy (EDS), to the task of identifying and characterizing the major phases which develop in austenitic stainless steels exposed to both thermal and radiation environments. By comparing the phase mixtures in thermal and radiation environments and the changes in phase chemistry, we are able to draw some conclusions regarding the relative importance of the various radiation induced phenomena.

Experimental

The data were derived from two types of austenitic stainless steels namely (a) AISI 316 and (b) titanium-stabilized versions of AISI 316. Several heats of each alloy were utilized in the course of this work. The chemical analyses of the heats examined fell within the ranges shown in Table I. These alloys were irradiated in both a solution annealed condition and in a 20% CW condition in the EBR-II fast reactor at Idaho Falls and also in the High Flux Isotope Reactor (HFIR) at Oak Ridge. The damage rate in both reactor experiments was $\cong 3 \times 10^{-5}$ dpa/s, however, the helium generated in these materials in HFIR was higher than that in EBR-II by a factor of $\sim 10^2$. In addition both alloys were irradiated with 4 MeV Ni ions at a damage rate of $\sim 5 \times 10^{-3}$ dpa/s after preinjection with 5 appm helium. Generally, specimens were in the form of 3 mm diam discs, 0.5 mm thick. Following irradiation or thermal aging, one surface of each TEM disc was electropolished using 10% perchloric-acetic acid to clean the surface. A carbon film 100–200 nm thick was then deposited on the clean surface, and the other side of the disc coated with lacquer. Using platinum tweezers to grip the sides, the disc was immersed in a 10% perchloric-10% glycerol-80% methyl alcohol (or 10% hydrochloric methanol) solution for one minute to allow electrolyte to penetrate to the polished surface before applying a current of 50 mA for two or three minutes to extract the carbon film. The film was floated off, washed in methyl alcohol, and retrieved on either a copper, beryllium, or carbon-coated vinyl grid. In this way a record of the phases present in each disc was retained

Table I. Alloy Compositions, wt %

Alloy	Fe	Cr	Ni	Mo	Mn	C	Ti	Si	P
316	Bal	16-18	12-14	2.2-2.6	1.5-2.0	.04-.06	<.05	.4-.8	.01-.03
316+Ti	Bal	14-17	12-16	2.0-2.5	1.5-2.0	.04-.06	.2-.25	.4-1.0	.01-.04

before proceeding with thinning and perforation. The extraction was used for chemical analysis of phases and for obtaining unambiguous single crystal diffraction patterns withoutmatrix double diffraction effects. Information on precipitate orientation relationships was obtained from examination of the thin foil. Most of the specimens were thinned by a drip electropolishing technique (1) or direct jet polishing (2). Other advantages from examining extracted phases are: (a) the gamma radiation from the highly radioactive matrix is eliminated; (b) x-ray signals from the matrix are eliminated; and (c) the microscope may be operated in the TEM mode rather than the STEM mode, thus minimizing carbon contamination which tends to impair sensitivity. A JEM-100CX microscope with an energy dispersive x-ray detector was used for TEM and microchemical analysis. The measured intensities were converted to compositional information after subtracting the hole count, employing the standardless approach outlined by Zaluzec (3). The data showed some scatter from particle to particle, and several particles were analyzed to get a statistical average. The precipitate phases which developed during alloy solidification or fabrication were often too thick to analyze by electron diffraction. These phases were extracted from the bulk material and mixed with TaC as an internal standard, and fixed on a Si-single crystal for x-ray analysis. Some of the bulk extracted precipitates were also embedded on a carbon film for EDS analysis and the electron beam focused at a thin edge of the particle to minimize absorption effect by the precipitate itself.

Results

In the following, each of the major phases observed is considered separately. The crystallography of each phase is described and previous observations briefly reviewed. Our own data is presented graphically to illustrate the temperature range over which the phase is observed in each environment, and also in tables to show the range of chemical compositions observed in wt %. Many of the irradiation experiments were carried out over restricted temperature ranges and thus the full extent of the temperature range of formation of a given phase is not often determined. This is indicated by broken lines in the diagrams. In a few instances it was possible to determine an approximate cut-off temperature for a phase, and this is indicated by a vertical bar.

The precision of an individual chemical analysis is largely determined by the counting statistics and decreases with decreasing elemental concentration because of the long counting times involved. In general, the accuracy of the measurements on individual particles is considered to be of the order of 1–2 wt %. In the microchemical analysis tables, the average elemental concentration is shown together with the range of observed values determined on a number of particles; usually between 2 and 10 particles were analyzed at a given irradiation temperature. Wider composition variations occur where data is reported for a range of irradiation temperatures.

Gamma Prime (γ') Phase

This phase has an ordered structure, $L1_2$, P_{m3m} with a lattice parameter $a_0 \sim 0.35$ nm. The stoichiometric atomic composition is Ni_3X where X typically is Al, Si, or Nb, although there is considerable solubility for other elements such as Ti, Fe, and Mo. This phase is a frequent component of stainless steels and nickel alloys in which the Ni concentration exceeds ~25 wt %, but it has never been observed to develop in thermally aged steels with Ni contents <20 wt %. However, formation of a γ' Ni_3Si compound during neutron irradiation was reported in stainless steels containing 13–14 wt % Ni both by Brager and Garner (4) and by Cawthorne and Brown (5). In the former case, γ' developed after irradiation of AISI 316 to 10 dpa at 427°C. With increasing fluence, γ' developed at increasingly higher temperatures with an upper temperature cutoff at 510–520°C. Similarly Cawthorne and Brown observed γ' formation in an M316 stainless steel irradiated in the Dounreay Fast Reactor. In this instance, precipitation was observed at temperatures as low as 270°C and at doses as low as 3 dpa. The upper cut-off temperature was 540°C.

Our own observations on γ' formation are summarized in Fig. 1. In both the AISI 316 and 316 + Ti steels, γ' was observed after irradiation in EBR-II to ~35 dpa over the range 400–510°C. In experiments conducted in HFIR, γ' was observed in AISI 316 irradiated to ~8 dpa over the range 300–400°C.

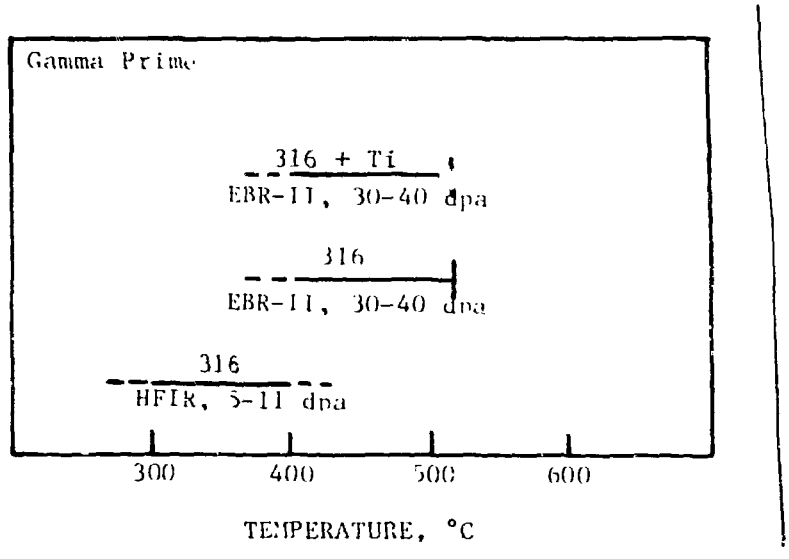

Fig. 1 - Temperature Range of γ' Formation.

Data on the chemical composition of γ' in the 316 + Ti irradiated in EBR-II to a dose of 35 dpa are presented in Table II. An example of a γ' particle EDS spectrum is presented in Fig. 2. Over the temperature range 427–482°C, the major components of γ' were Ni, Si, and Fe with minor amounts of Ti and Cr sometimes being detected. The average composition, in wt %, was 21Si-14Fe-64Ni and this composition agrees well with the average γ' composition determined by Brager and Garner (4). Thus the Si concentration in the γ' is higher than in the matrix by a factor of ~20 and Ni is enriched by a factor of ~4.

On an atomic basis, the ratio of all other atoms to Si, (M:Si), is only 1.5 at 427°C increasing to 2.0 at 454°C and 2.2 at 482°C. Thus in this alloy, the γ' phase is hyperstoichiometric with respect to Si but tends to

Table II. Microchemical Analysis of γ′, wt %

Alloy	Exposure Condition	Si	Mo	Ti	Cr	Mn	Fe	Ni
316 + Ti	EBR-II 35 dpa 427°C	23 22-25	--	--	--	--	11 11-12	65 64-66
316 + Ti	EBR-II 35 dpa 454°C	20 19-20	--	2 2-3	4 3-6	--	23 19-27	52 47-56
316 + Ti	EBR-II 35 dpa 482°C	18	--	--	--	--	8	74

ORNL-PHOTO 2887-80

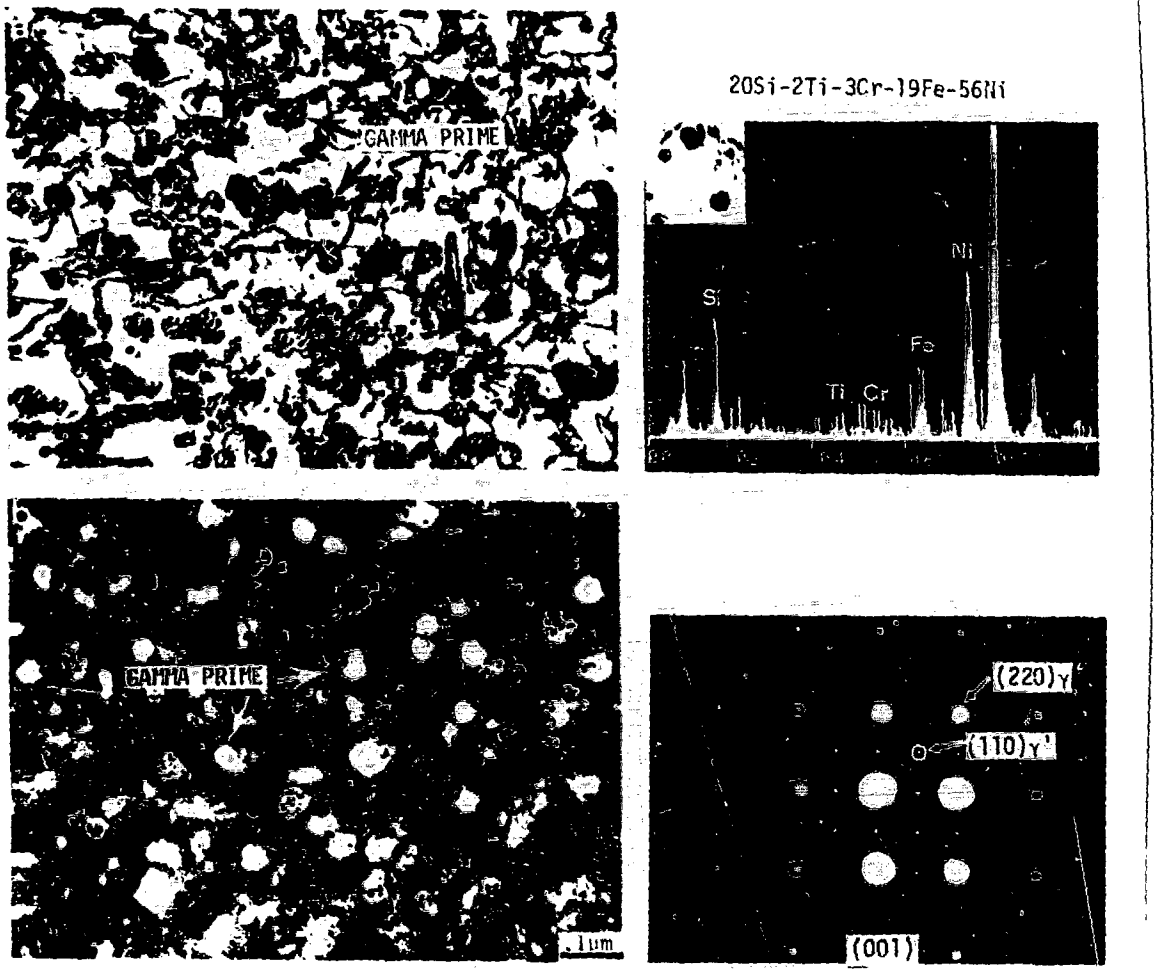

Fig. 2. Gamma Prime Precipitates in 316 + Ti Neutron Irradiated to 35 dpa at 454°C. (a) Bright Field and EDS Spectrum of Extracted Precipitates (Insert) and (b) (110)γ′ Dark Field and Corresponding Diffraction Pattern.

approach stoichiometry at higher temperatures. At all temperatures, nucleation of γ′ occurred at faulted Frank loops. At low fluences the loops were decorated with discrete particles which eventually coalesced to form a continuous ring of γ′. At this stage the loops were still faulted. With further

irradiation, the loops began to unfault and climb away from the γ' which eventually developed into an approximately spherical particle.

In the alloys examined here, γ' could not be detected after irradiation with 4MeV Ni ions over the range 525° to 750°C. However, Mazey et al (6) observed γ' formation in the range 525° to 575°C in stainless steels containing 0.5-1.4%Si following irradiation with 46MeV Ni ions.

G Phase

A large number of G phases exist having the general formula $T_6Ni_{16}Si_7$, where T is a transition element such as Ti, Mn, Cr, Zr, V, Ta, Hf, or Nb. These phases have the Th_6Mn_{23} cubic structure Al, Fm3m, with $a_o \sim 1.12$nm, and containing 116 atoms per unit cell (7). This type of phase has been observed to form during thermal aging of certain stainless steels and nickel alloys, e.g, Silcock (8) reported a $Zr_6Ni_{16}Si_7$ phase in a 25Ni 20Cr austenite aged at 950°-1150°C. G phase has never been observed, however in thermally aged AISI 316 or 316 + Ti. The development of a G phase in 316 + Ti alloys during neutron irradiation at 500°-600°C was first reported by Thomas (9).

Our observations on the occurrence of G phase are summarized in Fig. 3. G phase was observed over the range 400°-600°C in 316 + Ti irradiated in EBR-II to ~35 dpa, but was not observed in AISI 316 irradiated under similar conditions. G phase was not observed in either steel after irradiation in HFIR over the range 400°-700°C to doses of 60 dpa.

For irradiations carried out with 4MeV Ni ions on 316 + Ti, the temperature range for G phase formation was shifted upwards by ~200°C with the maximum volume fraction occurring at ~700°C. Data on the composition of the G phase is presented in Table III and a typical x-ray spectrum shown in Fig. 4. The average composition of the G phase formed during neutron irradiation between 400° and 550°C was 16Si-6Mo-2.5Ti-8Cr-7.5Mn-12Fe-48Ni. Compared to the initial average matrix composition this represented enrichment by a factor of 2-3 for Ni and Mo, a factor of ~4 for Mn and factors of ~10 and ~20 for Ti and Si respectively. G phase is impoverished in Fe and Cr with respect to the matrix. The range of concentrations observed is wide because the data includes measurements over a wide temperature range. There is in fact a pronounced tendency for the highest Cr and Mo concentrations to occur at the upper end of the temperature range and for the maximum Si concentrations to occur at ~450°C. An interesting feature is the strong partitioning of Mn to this phase. The presence of this element provides a unique "fingerprint" which allows rapid preliminary identification of G phase from examination of the x-ray spectrum. The composition of the G phase formed under ion irradiation was remarkably similar to that observed under neutron irradiation. During postirradiation annealing at the ion irradiation temperature, it was found that the G phase gradually dissolved. The composition measured after partial dissolution, Table III, indicates that during annealing, Si, Mn, and Ni diffused back into the matrix. The Fe, Cr, and Mo concentrations increased to the point where one might expect a transformation to Laves phase. However, the crystallography of the G phase persisted in spite of these major compositional changes.

Very little is known regarding the nucleation of G phase. For example, it is not known whether it is nucleated directly at interstitial loops or whether it develops from the transformation of another phase, e.g., γ'. Once nucleated, G phase develops into thick rods or blocky forms which do not exhibit a strong habit relationship with the matrix. The reasons for the absence of a strong parallel orientation relationship are not understood.

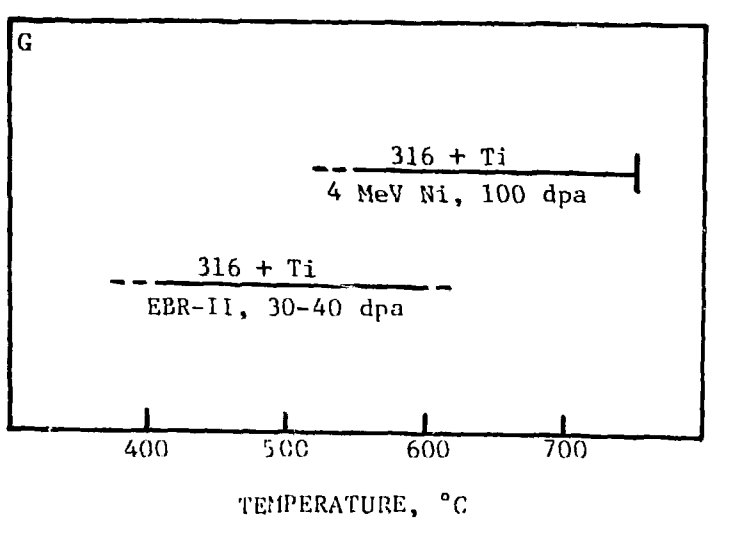

Fig. 3. Temperature Range of G Phase Formation.

Table III. Microchemical Analysis of G Phase, wt%

Alloy	Exposure Condition	Si	Mo	Ti	Cr	Mn	Fe	Ni
316 + Ti SA, CW	EBR-II 30-40 dpa 400-550°C	16 11-23	6 0-14	2 1-7	8 2-15	8 4-17	12 2-26	48 26-58
316 + Ti SA	4 MeV Ni Ion 70-100 dpa 675-700°C	21 19-22	5 4-6	4 3-5	8 6-9	5 4-5	9 8-9	51 48-53
316 + Ti SA	Same as above (4MeV $^{+}$Ni Ion) 6 h aged at 700°C	9	16	2	25	–	19	29

Eta phase (η). The structure of the eta phase was first described by Westgren (10) and reviewed later by Stadelmaier (11). The generic phase encompasses carbides, nitrides, oxides, and silicides. Two types of structure exist, namely, (a) the filled type, M_6X(X = C,N,O) and the unfilled type M_5SiX in which Si occupies a metal atom site and the X sites are vacant. The crystal structure of the eta phase is of the cubic, $E9_3$ Fd3m type with $a_o \sim 1.1$ nm and contains 96 atoms per unit cell.

Although the composition ranges and crystallography of the eta phases have been well documented, the occurence of a phase of this type in the 300 series stainless steels has not been well established because of its close similarity to the $M_{23}C_6$ phase. However, it was shown by Maziasz (12) that eta phase definitely develops in both annealed and 20% C.W. AISI 316 during thermal aging in the range 600°-650°C. The presence of eta phase in AISI 316 aged for long periods at 650°C was also reported by Bolten et al (13). It is highly probably that the presence of this phase has gone undetected in a considerable number of previously reported thermal aging experiments with stainless steels.

Our observations on eta phase formation are summarized in Fig. 5. In thermal aging experiments with AISI 316 over the range 500°-900°C, the formation of eta phase was confined to the region 600°-650°C. However,

ORNL-Photo 2674-80
21Si-6Mo-3Ti-9Cr-5Mn-8Fe-48Ni

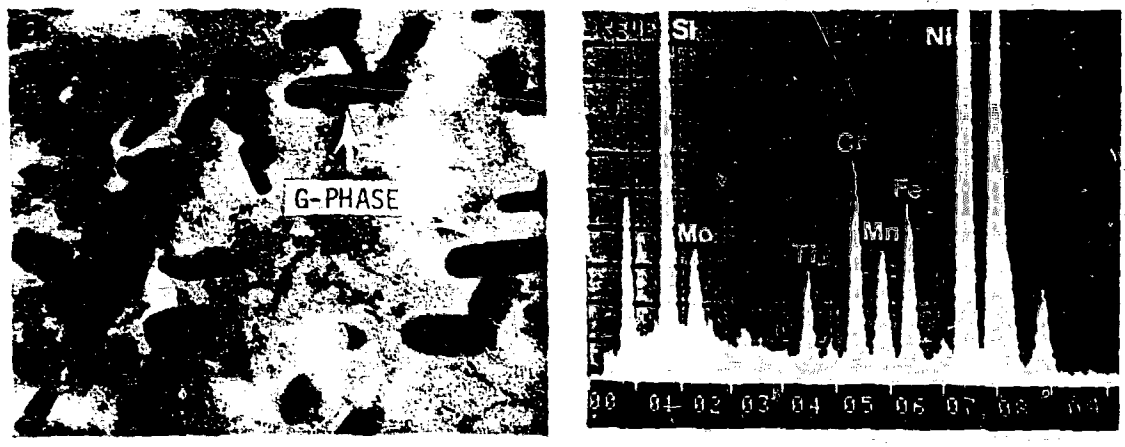

Fig. 4. G Phase in 316 + Ti Irradiated with 4 MeV Ni Ions at 700°C to 100 dpa and X-Ray Spectrum from Extracted Particle (insert).

during neutron irradiation significant precipitation occurred at much lower temperatures for comparable exposure times. Following irradiation in HFIR, eta phase was observed at temperatures down to 380°C with an upper cut-off at 550°C. In EBR-II irradiations, eta phase occurred over the range 400°-650°C with a maximum formation rate at 575°-600°C. For 316 + Ti similar temperature ranges of eta formation were observed for irradiations in both HFIR and EBR-II. During 4MeV Ni ion irradiation of AISI 316, very little precipitation occurred over the ranges 550°-700°C although the particles that did form were predominantly eta phase. In the 316 + Ti alloy, eta phase development was more pronounced and occurred at all ion irradiation temperatures from 550 to 700°C. Data on the chemical composition of extracted eta phase particles are shown in Table IV. For AISI 316 thermally aged at 600-650°C the average composition was found to be 7Si-23Mo-31Cr-11Fe-25Ni with minor amounts of Ti, Mn, and V. Compared with the initial matrix composition this represents an enrichment in Ni and Cr by factors of ∿2 and enrichment in Mo and Si by a factor of ∿10. Examination of eta phase particles extracted from AISI 316 after irradiation in EBR-II at 500°-600°C, Fig. 6, showed that the composition was very similar to that produced during thermal aging; further enrichment of Ni or Si was not observed. Furthermore, the composition of eta phase produced during HFIR irradiation at 370°-470°C was also essentially the same as that produced by thermal aging. The only difference was a significantly lower Mo concentration in the HFIR irradiation case, probably because of the reduced mobility of Mo at the lower temperatures of this experiment.

The fourth set of composition data is for the eta phase produced in 316 + Ti irradiated in EBR-II over the range 400°-600°C. The average composition was fully consistent with the other three sets of data. In this instance an effect of irradiation temperature was detected. As the irradiation temperature increased, the Ni and Cr concentrations in eta phase decreased steadily and the Mo concentration increased rapidly above 500°C. Maximum Si concentrations (∿10%) were observed at ∿450°C.

The composition of an eta phase which developed during 4MeV Ni ion irradiation at 600°-700°C of a 316 + Ti alloy (LSIA) was reported previously (14) as 9Si-7Mo-1Ti-32Cr-20Fe-31Ni . In spite of the higher damage rate and

temperature, this is fully consistent with the eta phase composition described above.

In summary, although the analyses of individual elements vary from particle to particle and also vary with irradiation temperature, the average eta phase composition is very similar in both thermal and irradiation environments and is also similar in both alloys. The general features are that compared to the matrix composition, the eta phase is enriched in Si, Mo, Cr, and Ni and is depleted in Fe.

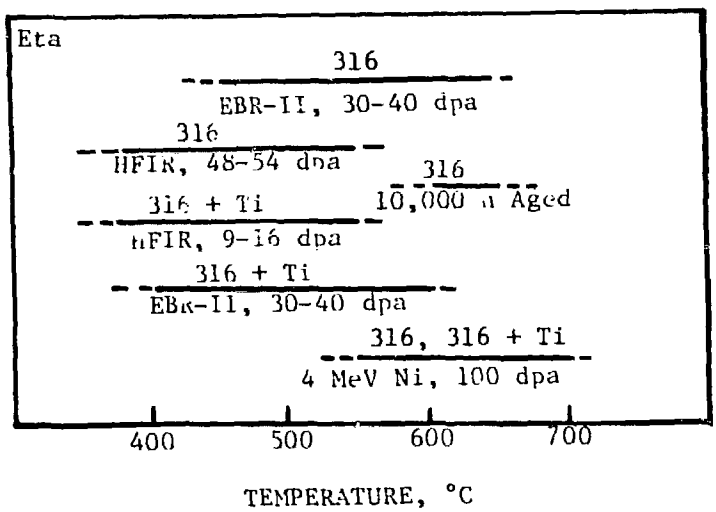

Fig. 5. Temperature Range of η Phase Formation.

Table IV. Microchemical Analysis of Eta Phase, wt%

Alloy	Exposure Conditions	Si	Mo	Ti	Cr	Mn	Fe	Ni	V
316	Thermal Aging 10,000h 600-650°C	7 4-9	23 15-35	.8 0-3	31 22-43	.8 0-3	11 3-25	25 14-31	1 0-6
316	EBR-II 30-40 dpa 500-600°C	7 6-7	17 14-20	---	32 31-32	---	15 14-15	30 27-33	---
316	HFIR 48-54 dpa 370-470°C	8 2-10	8 6-9	---	37 34-40	.4 .1-.8	17 14-22	29 28-31	2 1-3
316 + Ti	EBR-II 30-40 dpa 400-600°C	10 5-14	15 3-34	.4 0-2	30 19-39	---	17 11-19	28 18-36	---

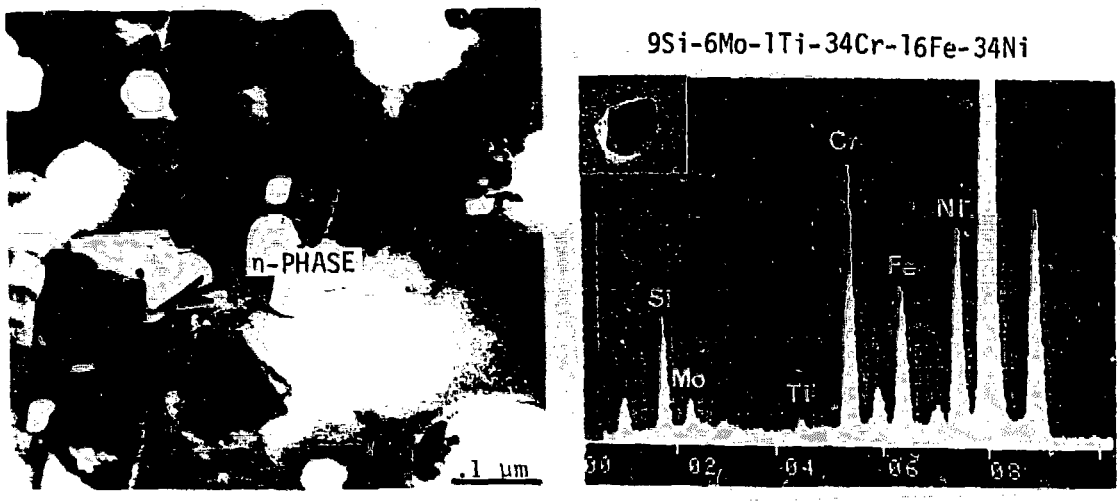

Fig. 6. η Phase in SA316 Neutron Irradiated to 35 dpa at 585°C in EBR-II and EDS Spectrum of Extracted Precipitate (Insert).

As with other phases, very little is known regarding the nucleation mechanism for eta phases. The majority of the particles develop a rhombohedral disc shape having either a cube-on-cube or a twin orientation relationship with the matrix. The morphology, lattice parameters, and crystal structure of the eta and $M_{23}C_6$ phases are very similar and distinction between the two phases requires careful diffraction analysis. On the basis of structure factor considerations, it is expected that the diffraction patterns from the diamond cubic eta phase would show systematic absences at (200), (420), etc. However, non-zero intensity frequently occurs for these reflections either as a result of ordering of atoms in the eta phase lattice or from double diffraction with matrix reflections. It has been found that the most satisfactory means of distinguishing between these phases is to extract particles on a carbon film and to tilt to an (001) zone axis. In this situation, although the forbidden eta phase reflections sometimes appear, they are of low intensity and are clearly distinguishable from the strong reflections from the $M_{23}C_6$ phase, Fig. 7. In addition, there are clear distinctions in phase chemistry which should be used to eliminate any remaining ambiguity.

$M_{23}C_6$ Phase

This phase is one of a large class of carbides and borides which fall into the category of tau phases. The $D8_4$, Fm3m structure is a complex cubic structure containing 92 atoms per unit cell and having a lattice parameter of ~1.06nm. A large number of metal atoms such as Fe, Mo, W, Ni, etc. can be substituted for Cr atoms. This phase is a frequent component of 300 series stainless aged in the temperature range 550°-900°C and its nucleation, composition, orientation relationship, and stability are well documented (15,16).

The development of $M_{23}C_6$ in two heats of AISI 316 during irradiation in EBR-II has been reported by Brager and Garner (4). They observed this phase over the temperature range 525°-610°C, the volume fraction increasing with irradiation temperature. Bramman et al (17) reported the development of this phase in 20% C.W. 316 fuel pin cladding over the range 400°-610°C. Because of the difficulties in positively identifying $M_{23}C_6$ (as described in the previous section), it is possible that some of the reported observations of $M_{23}C_6$ phase may be more correctly described as eta phase.

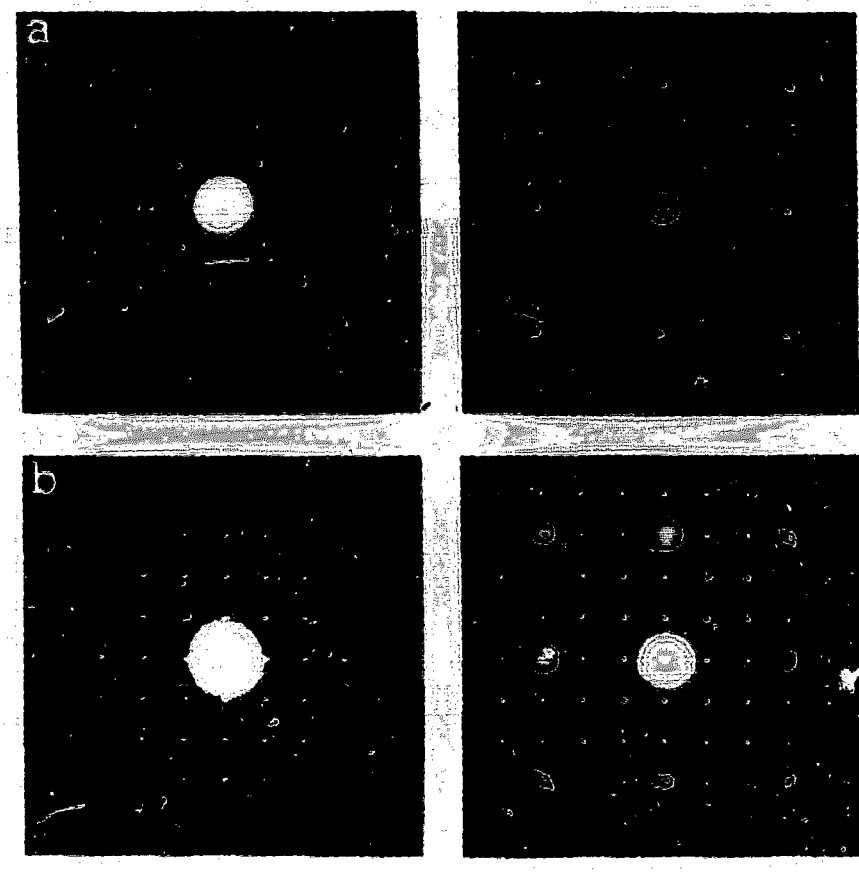

Fig. 7. (a) (001) Diffraction Patterns of η Phase on Extract Replica and in the Matrix. (b) (001) Diffraction Pattern of $M_{23}C_6$ on Extraction Replica and in the Matrix.

The temperature ranges of $M_{23}C_6$ formation in the present work are illustrated in Fig. 8. $M_{23}C_6$ developed in both AISI 316 and 316 + Ti during thermal aging over the range 550° to 850°C, the volume fraction being significantly lower in the latter alloy. This phase also developed, to a lesser extent, during irradiation of AISI 316 in both EBR-II and HFIR, primarily in the range 550°-600°C. Smaller amounts of $M_{23}C_6$ developed during neutron irradiation of 316 + Ti.

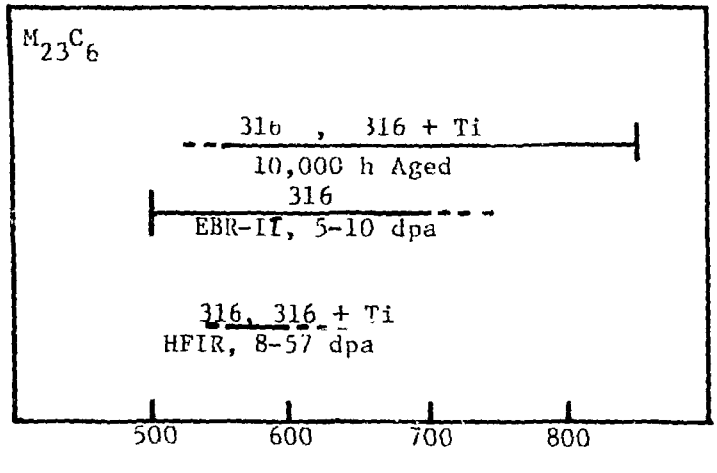

Fig. 8. Temperature Range of $M_{23}C_6$ Formation.

Our measurements on the composition of $M_{23}C_6$ are presented in Table V. In each case great care was taken to distinguish between this phase and eta phase since the two phases frequently coexist. After aging AISI 316 for 10,000 hr. at 600°-650°C, the average composition (wt%) of $M_{23}C_6$ was found to be 14Mo-65Cr-16Fe-4Ni, with minor concentrations of Si, Ti, and V. This composition represents an enrichment in Cr, and Mo compared to the initial matrix composition by factors of ∿4 and ∿7 respectively. This phase evidently rejects Ni strongly. Particles of $M_{23}C_6$ extracted from specimens of the same heat irradiated in EBR-II at 500°C were found to have essentially the same range of compositions. There was no significant enrichment in Ni and Si. The composition of $M_{23}C_6$ produced in 316 + Ti during HFIR irradiations at 600°C was very similar to the previous examples and recent data from thermally aged specimens also agrees well with those composition ranges.

In summary, although significant fluctuations in chemistry occur from particle to particle, the average chemistry of $M_{23}C_6$ is consistent for the two alloys examined after exposure to both thermal and irradiation environments. The general features are, that compared to the matrix, the $M_{23}C_6$ phase is enriched in Cr and Mo and is depleted in both Fe and Ni.

The effects of damage rate on the stability of $M_{23}C_6$ are not known since observations of this phase, confirmed by good diffraction evidence, are practically nonexistent. In our own ion irradiation studies with AISI 316 very little precipitation was ever observed between 525°C and 750°C. In 316 + Ti alloys, precipitation consisted mainly of G phase, and eta phase; the presence of $M_{23}C_6$ was never positively confirmed. Recently Williams et al (18) presented evidence for the precipitation of $M_{23}C_6$ during 4MeV Ni ion irradiation of FV 548 at 600°C.

Table V. Microchemical Analysis of $M_{23}C_6$, wt%

Alloy	Exposure Condition	Si	Mo	Ti	Cr	Mn	Fe	Ni	V
316 SA, CW	Thermal Aging 10,000 h 600-650°C	.5 0-2	4 9-20	.4 0-3	65 52-74	.5 0-2	16 8-27	4 1-9	.1 0-2
316 CW	EBR-II 6-11 dpa 500°C	2 1-3	12 11-13	.8 .4-1	56 54-59	2 .2-3	20 13-25	7 4-12	1 .4-1
316 + Ti SA	HFIR 30 dpa 600°C	1 .5-1	11 10-11	.3 0-.6	60 56-65	---	22 18-26	5 4-5	1 0-2

The chemical composition of $M_{23}C_6$ phase is evidently very different from that of the structurally similar eta phase and the differences in x-ray spectra present a useful "fingerprint" for rapid phase identification. An example of this technique is shown in Figure 10.in which the two phases not only coexist but appear to have nucleated sympathetically during aging at 600°C. This situation presents a particularly difficult situation for identification by SAD. The EDS anaylsis, however, clearly distinguishes between the two phases with the eta phase exhibiting strong Ni and Si peaks.

Fig. 9. Extracted $M_{23}C_6$ and η Phase Particles in CW 316 Aged at 600°C for 10,000 h. Analyses shown are for the individual particles.

The orientation relationship between the $M_{23}C_6$ phase and the matrix was predominantly cube-on-cube although twinned relationships were also frequently observed. Particles developed as rhombohedral plates or laths.

Laves Phase

A large number of intermetallic phases of general formula AB_2 have been classified as Laves phases following the original work on this subject by Laves, Witte, and their associates (19,20). There are three prototypic Laves structure types, namely Zn_2Mg (hexagonal), Cu_2Mg (cubic) and Ni_2Mg (hexagonal). A Laves phase Fe_2Mo has been observed frequently in stainless steels containing Mo, and its formation has been reviewed by Weiss and Stickler (15). In their own work these authors observed Laves phase in AISI 316 aged over the temperature range 600°-815°C. They showed that this phase was of the Zn_2Mg type C14, $P6_3/mmc$ containing primarily Fe and Mo with lesser amounts of Ni and Cr, and with lattice parameters $a_o \sim 0.88$ nm and $c_o \sim 0.46$ nm.

Our observations on the temperature ranges for Laves formation are summarized in Figure 10. In the 316 + Ti alloy Laves developed during thermal aging over the range 650°-750°C, the solvus temperature for this phase being ~850°C. In AISI 316 Laves formation was observed after 10,000 hr at 600°C. During neutron irradiation in both EBR-II and HFIR, the volume fraction of Laves phase was greater and precipitation occurred at significantly lower temperatures, i.e., down to 500°C.

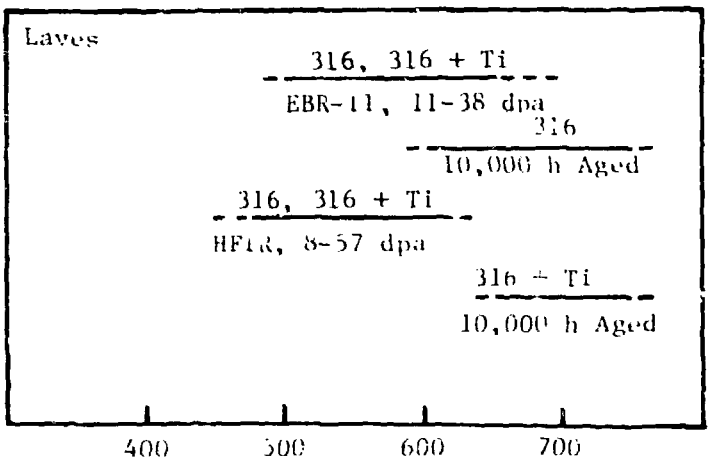

Fig. 10. Temperature Range of Laves Formation.

Laves phase was not observed in either AISI 316 or 316 + Ti irradiated with 4MeV Ni ions to a dose of 100 dpa over the range 525°-750°C. The stability of Laves phase during Ni ion irradiation was further examined in an experiment in which 316 + Ti was initially irradiated in EBR-II at 600°C to a dose of ~10 dpa. During subsequent irradiation with 4MeV Ni ions at 675°C, the Laves phase produced during the neutron irradiation dissolved and was replaced by G phase.

Data on the composition of the Laves phase is presented in Table VI, and a typical x-ray spectrum shown in Fig. 11. The phase which developed during thermal aging of AISI 316 was composed mainly of Fe, Mo, and Cr with smaller amounts of Ni and Si, the average composition being 5Si-43Mo-13Cr-33Fe-5Ni. An almost identical composition was found for Laves phase in AISI 316 after irradiation in HFIR at 550°C. However, during HFIR irradiation at a lower temperature (470°C), the Laves phase became significantly enriched in Ni (22%), the Mo content being correspondingly reduced (16%). The Laves phase which developed in AISI 316 irradiated in EBR-II at temperatures between 500° and 600°C was also enriched in Ni and had an average composition of 9Si-23Mo-13Cr-24Fe-31Ni.

In the 316 + Ti alloy irradiated in HFIR at 600°C, the composition of Laves was approximately the same as that observed in AISI 316 irradiated under the same conditions. For the 316 + Ti alloy irradiated in EBR-II, data was obtained at 4 different temperatures between 500° and 650°C, and it was possible to discern some distinct trends in composition with temperature. It was found that the average Mo concentration increased from ~12% at 500°C to ~30% at 650°C, while over the same temperature range the Ni content decreased from ~30% to ~12%. Both Cr and Si concentrations remained fairly constant with temperature.

In summary, it has been observed that under thermal aging conditions, the Laves phase is highly enriched in Mo and rejects Ni quite strongly. Significantly, the average Si content is a factor of ~6 higher than the average

initial matrix content. The Laves composition is unaffected by high temperature HFIR irradiation, but significant enrichment in Ni occurs at an irradiation temperature of ~470°C. The same trend toward increasing Ni enrichment with decreasing temperature occurs in EBR-II. For irradiation at ~550°C there appears to be significantly higher enrichment factors for both Ni and Si in EBR-II than in HFIR.

Table VI. Microchemical Analysis of Laves Phase, wt%

Alloy	Exposure Condition	Si	Mo	Ti	Cr	Mn	Fe	Ni	V
316 SA, CW	Thermal Aging 10,000 h 600-650°C	5 1-7	43 38-39	---	13 4-16	1 0-2	33 17-37	6 3-7	.2 0-1
316 SA	HFIR 42 dpa 550°C	5	42	--	13	.4	31	7	1
316 CW	HFIR 54 dpa 470°C	3 2-4	16 13-19	.7	24 22-26	11 11	32 31-32	22 21-32	3 2-3
316 SA	EBR-II 30-40 dpa 500-600°C	10 9-10	23 22-24	---	13 12-13	---	24 23-25	31 29-33	---
316 + Ti	HFIR 30 dpa 600°C	4 4-5	31 30-33	1 .6-2	16 15-17	.5 .2-.8	35 34-40	8 7-10	1 .9-2
316 + Ti SA,CW	EBR-II 30-40 dpa 500-650°C	9 6-15	24 8-31	.7 0-3	15 11-23	.5 0-4	30 17-39	21 10-42	---

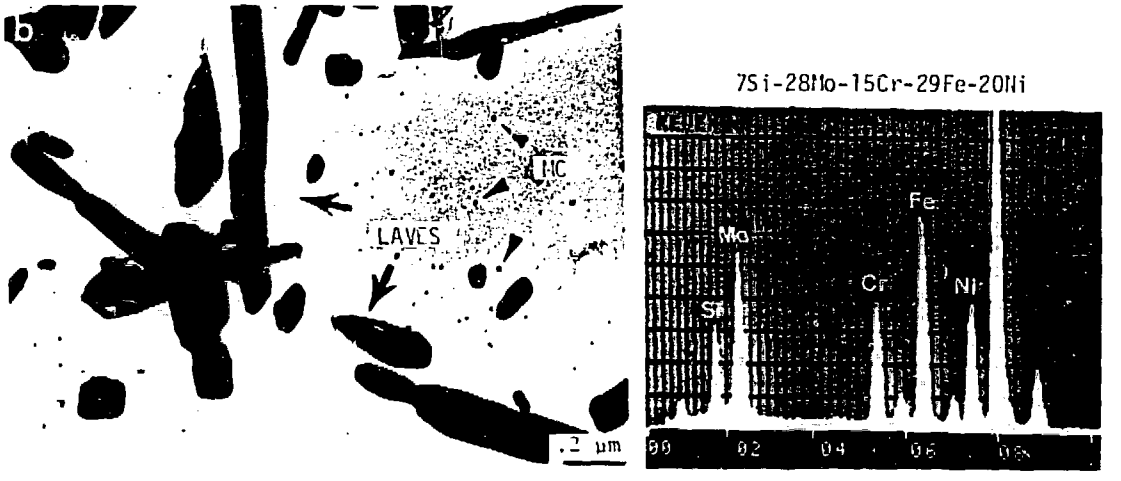

Fig. 11. Laves Phase in 316 + Ti Neutron Irradiated to 35 dpa at 590°C and X-Ray Spectrum from Extracted Particle.

The Laves phase develops into both globular and lath-shaped particles; the latter invariably contain internal faults which give rise to characteristic streaks in diffraction patterns. Although several orientation relationships between Laves and austenite have been reported. The number of variants is so large that Laves particles appear to be randomly oriented with respect to the matrix.

Chi Phase (χ)

Chi phase is an Fe-Cr-Mo compound, chemically and structurally related to σ phase, which was first detected by Andrews and Brookes in thermally aged steels containing Mo. (21). This phase was subsequently shown to possess an ordered B.C.C., γ-Mn Al2 structure having 58 atoms per unit cell and with $a_o \sim 0.88$nm (22). It is believed to be a carbon-dissolving compound. Its formation in AISI 316 stainless steel has been reviewed by Weiss and Stickler (15). In their study, chi phase was generally found in the same temperature range as sigma, and frequently preceded the formation of sigma. The composition in wt% was found to be 22Mo-21Cr-52Fe-5Ni. Our own limited observations of chi phase are summarized in Figure 12. Minor quantities of this phase were observed in AISI 316 aged at temperatures from 700° to 850°C and also in a 316 + Ti alloy aged 750°C. A limited amount of chi phase was observed in both AISI 316 and 316 + Ti irradiated in HFIR at 650°C.

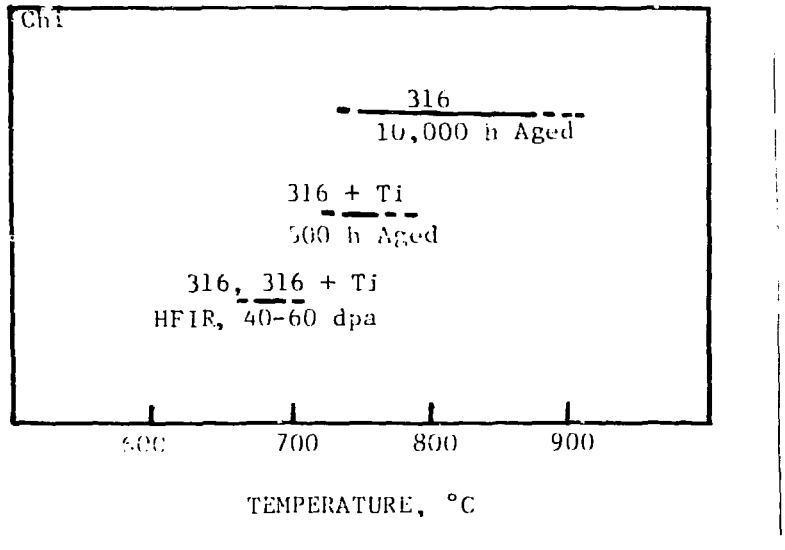

Fig. 12. Temperature Range of Chi Phase Formation.

Sigma Phase (σ)

The sigma phase classification encompasses an extremely wide range of compounds containing one element from Group VA or VIA with a second element from the First, Second, or Third Long Period. The crystal structure is tetragonal, $D8_b$, P4/mnm with $c/a \sim 0.52$, and 30 atoms per unit cell. The sigma phase FeCr is frequently observed in 300 series austenitic steels containing >14% Cr during thermal aging at 650°-850°C and its formation is generally accelerated by the additions of Ti or Mo. Sigma formation

in binary, ternary, and complex alloy systems has been reviewed by Hall and Algie (23). Time-temperature precipitation diagrams for the formation of a sigma phase in AISI 316 stainless steel have been presented by Weiss and Stickler (15).

Our observations on sigma phase development are summarized in Figure 13. During thermal aging, this phase developed in both AISI 316 and 316 + Ti steels over the temperature range 600°-900°C. For both alloys, the rate of sigma formation was enhanced by neutron irradiation and the temperature range extended downwards to 550°C. Sigma phase formation was not observed during irradiation with 4MeV Ni ions. An example of a σ phase diffraction pattern and x-ray spectrum is shown in Figure 14. The only chemistry data presently available is for specimens thermally aged at 650°C. The average composition was found to be 1.4Si-6Mo-37Cr-50Fe-5Ni, which is in good agreement with the composition reported by Weiss and Stickler (15).

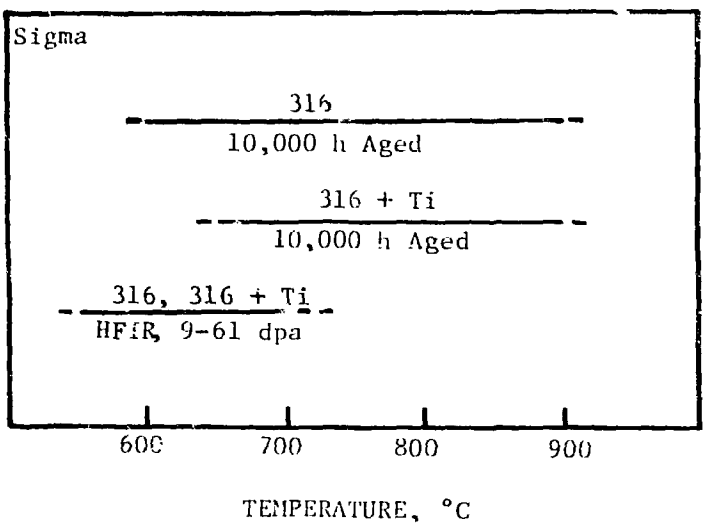

Fig. 13. Temperature Range of Sigma Phase Formation.

MC Phase

The MC carbides have a cubic structure, type B1, F_{m3m} with four metal atoms per unit cell and lattice parameter $a_o \sim 0.43$nm. M refers to any of the transition elements Ti, Zr, Hf, V, Nb, or Ta. These compounds exist over a range of stoichiometry and frequently dissolve other elements such as Mo. Precipitation of MC carbides occurs in stabilized stainless steels during thermal aging between 600° and 1050°C and the subject has been reviewed extensively (16, 24).

The temperature ranges over which TiC precipitation was observed in various environments are illustrated in Figure 15. During thermal aging of 316 + Ti alloys, precipitation of TiC occurred at temperatures from ~600°C up to the solvus temperature at ~1100°C; precipitation was particularly rapid over the range 750°-850°C. During neutron irradiation in EBR-II, precipitation of TiC was observed from 510°C up to the highest temperature investigated, i.e., 650°C. The absence of TiC at lower irradiation temperatures does not appear to be a kinetic problem. When TiC was precipitated prior to irradiation by cold working and aging, dissolution occurred during subsequent irradiation in EBR-II at temperatures at or below 500°C. This low temperature instability may be related to the rapid development of G phase which occurs in this temperature range. In contrast to this behavior, precipitation of TiC was observed in heats of 316 + Ti irradiated in HFIR at temperatures as low as 280°C.

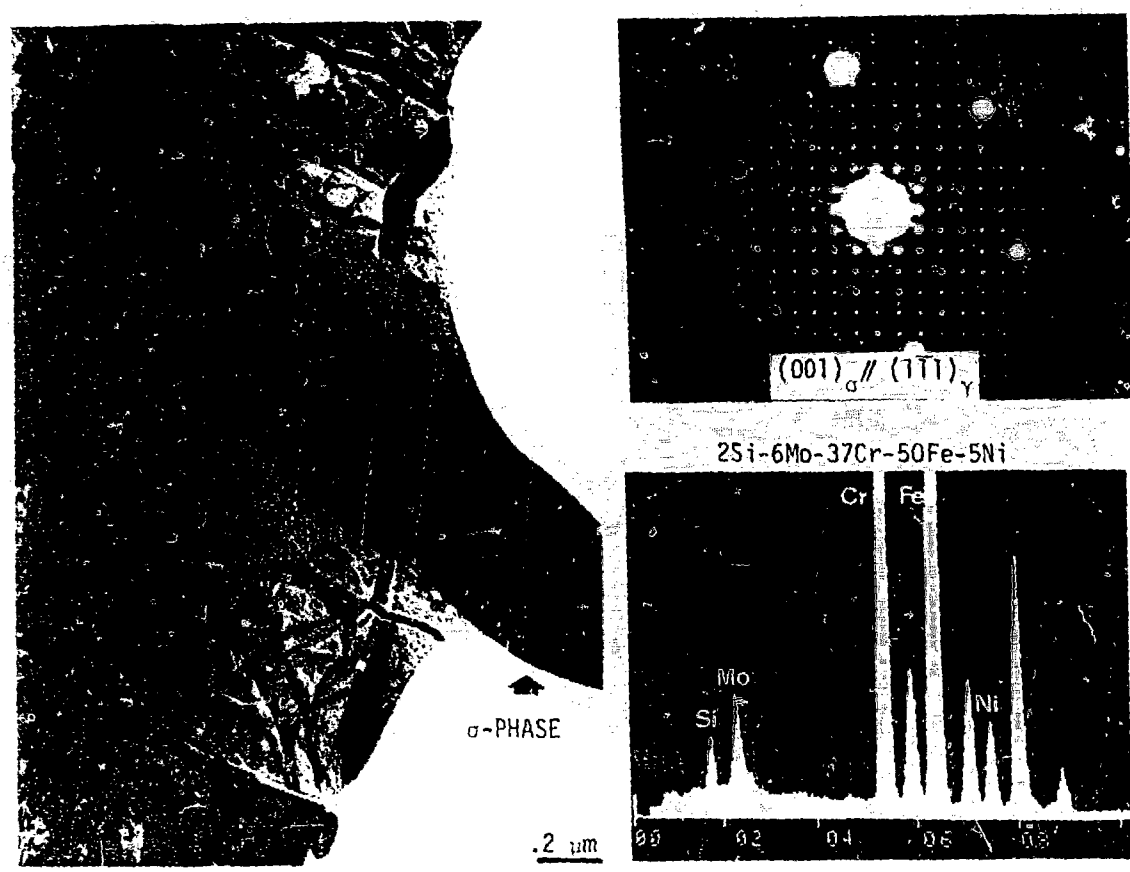

Fig. 14. σ Phase in CW 316 Thermally Aged for 10,000 hours at 650°C.

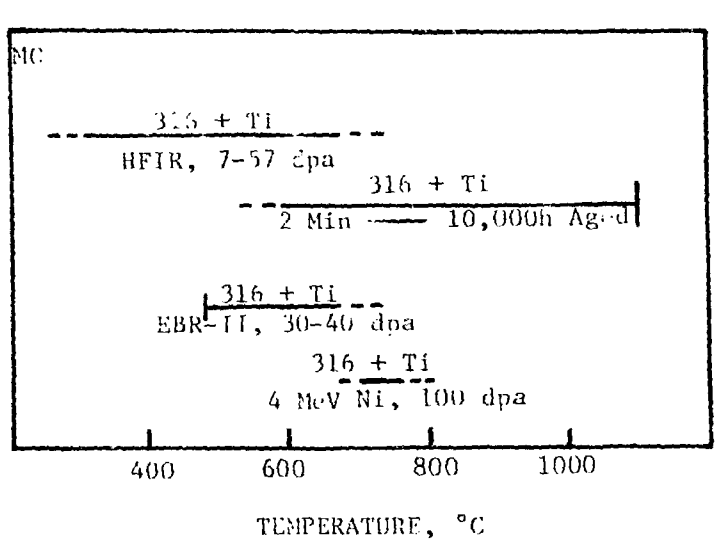

Fig. 15. Temperature Range of MC Formation.

Precipitation of TiC during 4MeV Ni ion irradiation was limited to the temperature range 700°-750°C and only occurred in heats of 316 + Ti in which G phase formation was restricted. Whenever G phase was the dominant mode of precipitation, TiC precipitation was suppressed well below the volume fraction which develops in an equivalent thermal aging treatment.

Data on the composition of the MC phase are presented in Table VII and a typical EDS spectrum is shown in Figure 16. Large concentrations of Mo were present in specimens annealed at 1050°C, together with smaller amounts of Fe and Cr. The presence of Si was not detected. The residual elements V and Nb which are normally present at levels of 50–100 ppm coprecipitated with Ti and reached concentrations of several wt% in the MC phase. Particles which precipitated during irradiation of the same heat in HFIR at 600°C contained a significantly higher proportion of Mo and in fact Ti and Mo were present in approximately equal amounts. The third set of data shown in Table VII is for 316 + Ti irradiated in EBR-II at 500–650°C. Again, Mo was a major constituent ranging from 8 to 30%, and in this material; significant quantities of Ni and Si were also present in some particles.

ORNL Photo 4168-80

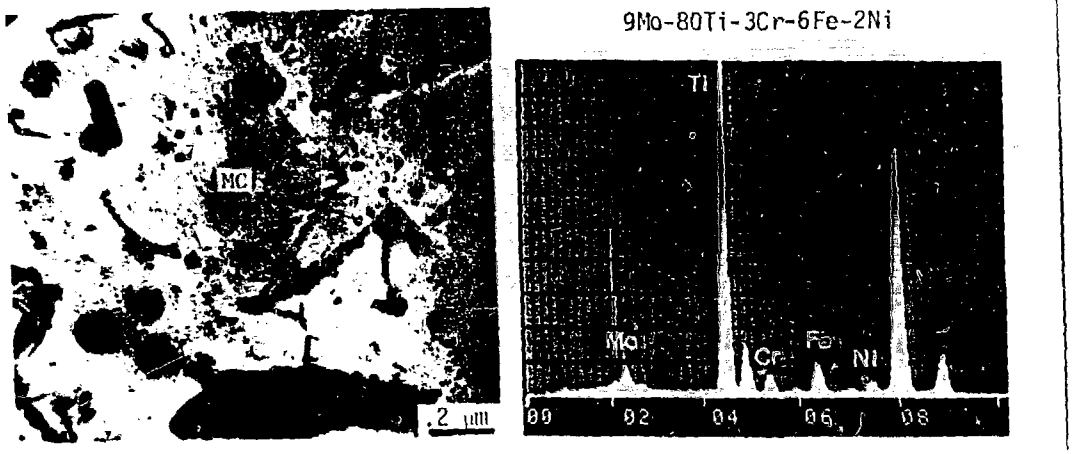

Fig. 16. MC Phase in 316 + Ti Neutron Irradiated to 35 dpa at 650°C and X-Ray Spectrum from Extracted Particle.

Table VII. Microchemical Analysis of MC Particles, wt%

Alloy	Exposure Condition	Si	Mo	Ti	Cr	Mn	Fe	Ni	V	Nb
316 + Ti	Thermal Aging 1050°C/1h	---	20 16-24	66 62-69	1 .4-2	---	1 0-2	.3 0-.8	3 2-3	9 7-10
316 + Ti	HFIR 30 dpa 600°C	.4 0-1	38 33-44	37 30-46	6 3-7	.2 0-1	8 5-11	3 1-6	7 5-8	2 0-5
316 + Ti	EBR-II 30-40 dpa 500-650°C	3 0-4	16 8-30	62 55-80	4 0-7	---	6 0-11	9 0-19	---	---

The large misfit strain between MC and the austenite matrix may be relieved by dislocation punching or by a flow of vacancies. Several nucleation mechanisms exist for MC, each associated with a different mechanism for the relief of misfit strain, e.g., decoration of dislocations; planar aggregates on [100] planes as a result of repeated nucleation on climbing dislocations; repeated nucleation on a climbing Frank partial; strings of particles in <100> directions; precipitation of uniform dispersions on vacancy clusters. Normally TiC develops with a cube-on-cube orientation with the matrix. Recently, however, a new morphology and habit was observed (30). During high temperature thermal aging and during HFIR irradiation of several heats of 316 + Ti, a rod morphology was observed with the rod axis along $[\bar{1}10]_{TiC} // [\bar{1}10]_{\gamma}$. The crystal habit was found to be close to the twin relationship for FCC crystals.

Iron Phosphide (Fe_2P)

The structure of the large class of binary transition metal phosphides has been reviewed by Rundqvist (31). The existence of phases of this type in austenitic stainless steel with normal levels of phosphorus has been reported recently. Bentley and Leitnaker (32) reported a needle-shaped hexagonal phase (a_o = .608 nm, c_o = .364 nm) growing in <001> directions in AISI 321 stainless steel which had been aged for 17 years at ~600°C. Precipitation of a phosphide phase in an 18Cr-10Ni stainless steel containing 0.3 wt % P was described by Rowcliffe and Nicholson (33).

In the present work, although Fe_2P was not observed in thermal aging experiments, it was observed in both AISI 316 and 316 + Ti irradiated in EBR-II, Fig. 17. In solution annealed AISI 316, needle-shaped particles tentatively identified as the phosphide phase, developed during irradiation over the range 500–625°C. This phase was not observed in the cold-worked condition. In a heat of 316 + Ti containing .04 wt % P, the phosphide phase was the dominant mode of precipitation at 600°C, Fig. 18. This precipitate was identified as a hexagonal phase with a_o = 0.604 nm and c_o = .360 nm. The particles adopted a thin lath morphology with rapid growth occurring along $<001>_{\gamma}$ direction as a result of close matching with the particle c-axis direction. The orientation relationship was $(0001)_{Fe_2P} // (001)_{\gamma}$ and $(1210)_{Fe_2P} // (110)_{\gamma}$; consistent with the observations of Bentley and Leitnaker (32). A limited number of analyses were obtained from extracted particles and an example of an EDS spectrum is shown in Fig. 18. The average composition was found to be 16Si-19Cr-29Fe-27Ni-5P-4S. Thus, Si, P, and S are all highly enriched in this phase. In comparison, the composition of

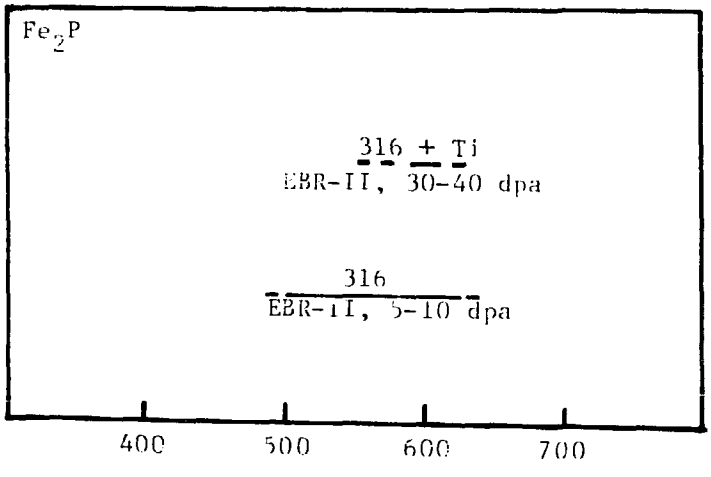

Fig. 17. Temperature Range of Fe_2P Formation.

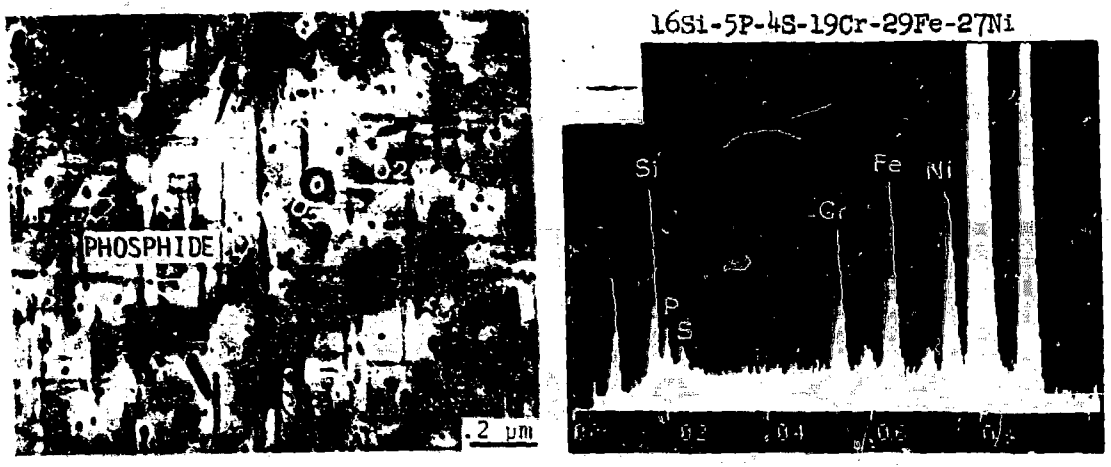

Fig. 18. Fe_2P Phase in 316 + Ti Neutron Irradiated to 35 dpa at 600°C (Z = $[001]_\gamma$) and X-Ray Spectrum from Extracted Particle.

the phase observed by Bentley and Leitnaker was 27Ti-4Cr-27Fe-17Ni-7P-18As. In spite of the compositional differences, the crystal structure, lattice parameters, and morphology are sufficiently similar to justify classifying both phases as belonging to the Fe_2P type.

Phases Formed During Alloy Fabrication

Under this heading, we include all the oxides, sulphides, nitrides, and other compounds which are formed either during alloy melting and solidification, or during high temperature fabrication. The number of such phases is surprisingly large and data are presented on six phases which have been identified in Ti-modified stainless steels. These particles are generally fairly large and frequently become stringered during rolling operations.

The compositions of these phases are presented in Table VIII. The phases ZrO and $Zr_4C_2S_2$ were detected in heats containing as little as 0.02 wt % Zr. Both phases were notable for containing high concentrations of Ti. The 316 + Ti contained TiN and this phase did not appear to dissolve other elements. The volume fraction of these compounds depends upon the levels of Zr, O, and N impurities in the steel. Their formation is significant because to some extent, the volume fraction of these phases affects the amount of free Ti available for precipitation reactions during aging. Three other compounds were frequently detected, namely, (a) a titanium carbonitride rich in S, (b) an unidentified Ti compound containing Mn, and (c) an unidentified compound rich in Si and Mn.

Discussion

A total of nine phases have been identified which precipitate from the austenite solid solution during exposure to thermal or irradiation environments. In addition minor quantities of at least three other phases which precipitate during alloy solidification or high temperature fabrication have been identified. For convenience, the crystallographic data on these phases are summarized in Table IX. Data is continually being accumulated from various irradiation and aging studies which will eventually allow us to develop time-temperature-precipitation diagrams for these phases in both thermal and irradiation environments. It will then be possible to attempt quantitative analysis of

TABLE IX

SUMMARY OF CRYSTALLOGRAPHIC DATA OF PRECIPITATE PHASES

PHASES	CRYSTAL STRUCTURE	LATTICE PARAMETER (nm)	SOLUTE ATOMS PER UNIT CELL	TYPICAL MORPHOLOGY	ORIENTATION TO γ-MATRIX
γ	Cubic, A1, Fm3m	a_0 = 0.36	4	Matrix	—
γ'	Cubic, $L1_2$, Fm3m	a_0 = 0.35	4	Small Sphere	Cube-on-Cube
G	Cubic, A1, Fm3m	a_0 = 1.12	116	Small Rod	Random
Fe_2P	Hex., C_{22}, P_{321}	a_0 = 0.604 c_0 = 0.36	6	Thin Lath	$(1\bar{2}10)_{ppt}$// $(011)_\gamma$ $(0001)_{ppt}$// $(001)_\gamma$
η	Cubic, $E9_3$, Fd3m	a_0 = 1.08	96	Rhombohedral	Cube-on-Cube or Twin
Laves	Hex., C14, $P6_3/mmc$	a_0 = 0.47 c_0 = 0.77	12	Faulted Lath	Many Variants
$M_{23}C_6$	Cubic, $D8_4$, Fm3m	a_0 = 1.06	92	Rhombohedral Platelet	Cube-on-Cube or Twin
MC	Cubic, B1, Fm3m	a_0 = 0.433	4	Small Sphere	Cube-on-Cube
σ	Tet., $D8_b$, P4/mnm	a_0 = 0.88 c_0 = 0.46	30	Various	Many Variants
χ	Cubic, A12, $I\bar{4}3m$	a_0 = 0.89	58	Various	Many Variants
TiN	Cubic, B1, Fm3m	a_0 = 0.425	4	Large Cuboid	
$Zr_4C_2S_2$	Hex., $P6_3/mmc$	a_0 = 0.34 c_0 = 1.21		Globular	
ZrO	Cubic, B1, Fm3m	a_0 = 0.46	4	Globular	

Table VIII. Microchemical Analysis of Insoluble Phases, wt%

Phases	Si	Mo	Ti	Cr	Mn	Fe	Ni	Other Elements
$Zr_4C_2S_2$	---	---	40 26-53	---	---	---	---	Zr 41(22-59) S 20(15-25)
ZrO	3 0-8	---	21 5-33	2 1-4	1 .6-2	9 5-14	7 2-15	Zr 57(42-65)
TiN	---	---	-100-	---	---	---	---	----------
Si-Rich	35 30-39	--	17 9-25	7 6-8	41 37-45	--	---	----------
Ti-Rich	---	---	-82-	-6-	-12-	--	---	----------
Ti(C,N S	---	2 1-2	60 55-65	3 .4-5	.2 0-.4	8 1-15	1 0-2	V 3(2-4) Nb 2(1-2) S 22(19-25)

the effects of irradiation on phase stability in these complex alloys. However, even from the present data it is possible to discern the major effects of radiation on the phase relationships in 316 and 316 + Ti alloys. One of the striking features of this work is that detailed TEM examination of alloys irradiated in two reactor environments and also with 4 MeV Ni ions did not reveal any new phases. All the phases identified have also been observed in thermal aging studies. However, the appearance of two of the phases identified, namely γ' and G, was totally unexpected in the alloy compositions being studied. Both of these phases are characteristic of ternary or quarternary systems far removed from the base compositions of the 316 and 316 + Ti stainless steels. These phases are termed radiation-induced since (a) they cannot be produced by thermal aging of the alloy composition being considered and (b) they undergo reversion during postirradiation annealing at the irradiation temperature.

A second irradiation effect manifest in this work is an increase in the kinetics of precipitation of certain phases. Thus it has been observed that for comparable exposure times and temperatures the volume fraction of a phase is higher in the irradiation environment. In addition, for similar exposure times, appreciable precipitation of certain phases sometimes occurs at lower temperatures in a neutron-irradiation environment. This is termed radiation-enhanced precipitation.

The application of x-ray microanalytical techniques in phase identification has revealed a third major irradiation effect. Each of the phases examined accommodates a wide variety of atomic species and may encompass a surprisingly wide range of atomic proportions; particle to particle variations of a factor of $\sim$2 in a given elemental concentration are not uncommon. However, for some phases, the average composition which develops during irradiation differs markedly from that produced during thermal aging, principally because of the incorporation of substantial concentrations of Ni and/or Si. Such phases are termed radiation-modified.

The modifications to precipitation behavior described above appear to be primarily governed by radiation-enhanced diffusion and radiation-induced segregation. Many precipitation reactions in the austenitic

stainless steels are sluggish at temperatures below 600°C and extremely long aging times are required to approach equilibrium. Because of the enhanced point defect concentrations, the diffusion coefficients of solute and solvent atoms may be increased by several orders of magnitude particularly during neutron irradiation at temperatures below ∿550°C (34). Precipitation of phases which depend upon concentrations of Fe, Cr, and Mo for their development are frequently enhanced because of increased atomic mobility.

High temperature irradiation induces fluxes of interstitial and vacancy-type defects to internal sinks such as dislocations, grain boundaries, voids, and interfaces. When migration of either defect type occurs by preferential association with selected solute species, a coupled net flux of solutes to point defect sinks develops. It is well established that such radiation-induced segregation provides a powerful mechanism for transporting sufficient solute to change local concentrations of solute by several orders of magnitude (35).

It has been shown that in the binary Ni-Si system, Si atoms are preferentially transported to sinks through the rapid migration of silicon-defect complexes (36–38). It has also been shown that during the irradiation of Fe-Cr-Ni ternary alloys, Ni becomes enriched at sinks (39,40) possibly because Ni is the slowest diffusing component of this system.

These solute transport mechanisms also operate in complex alloys. For example, Kenik (41) has detected the segregation of Si to interstitial loops in a Ti-modified stainless steel irradiated with Ni ions. In addition, Marwick et al. (42) observed that Ni segregates strongly to void surfaces in a complex Ni alloy during ion irradiation. The radiation-induced phases, G and γ', are characterized by high concentrations of Ni and Si suggesting that the transport of these elements along point defect gradients is a dominant factor in the nucleation of these phases. Nucleation occurs when a critical concentration is exceeded by segregation to a loop. The creation of a particle-matrix interface which provides sites for point defect recombination ensures a continued flow of solute to the embryonic particle.

The phases which develop during thermal aging also develop during irradiation. Their interfaces provide sites for point defect annihilation and large point defect gradients are set up. Phases with a negative volumetric mismatch with respect to the matrix will tend to have a bias for interstitials and hence the solute flux will be biased towards those atomic species preferentially migrating by an interstitial mechanism. The converse is true for phases with a positive mismatch. Thus the sense of the volumetric mismatch influences the proportions of atomic species ariving at the interface. For both types of phases the net flux is different from that which develops in a thermal environment both in magnitude and in composition. Whether or not the composition of a given phase is modified by radiation depends upon whether or not there is appreciable solubility for the preferentially migrating species. For example, Ni is soluble in Laves phase and during irradiation a modified Ni-rich Laves phase develops. On the other hand, phases such as $M_{23}C_6$ and MC essentially reject the additional components of the radiation-induced atomic flux and absorb the same proportions of elements as they absorb in a thermal environment; they are enhanced, but not modified.

The principle phases observed in the neutron irradiated 316 and 316 + Ti alloys may be categorized in terms of the preceding discussion as follows:

(a) γ' phase: radiation-induced, enriched in Ni, Si. Reversion of this phase during postirradiation annealing was demonstrated by Brager and Garner (43).

(b) G phase: radiation induced, enriched in Ni, Si, Ti, and Mn. Reversion of the G phase produced by Ni ion irradiation of 316 + Ti was described in the previous section.

(c) η phase: radiation-enhanced, but not modified. Enriched in Ni and Si as well as Mo and Cr during thermal aging. Essentially the same composition develops during neutron irradiation.

(d) $M_{23}C_6$ phase: neither enhanced or modified. Enriched in Mo and Cr. Approximately the same compositions and volume fractions were observed in thermal and irradiation environments.

(e) Laves phase: radiation-enhanced and modified. Enriched in Mo and Si and rejects Ni during thermal aging. During neutron irradiation, Ni is accommodated, the proportion of Ni increasing as the irradiation temperature decreases.

(f) MC phase: Enhanced but not modified. Enriched in Ti and Mo and rejects Ni in both thermal and radiation environments. May be suppressed under conditions favorable for G phase formation.

(g) σ and Fe_2P phases: There is presently insufficient data to categorize these phases. There is some evidence that σ phase formation is enhanced by irradiation in HFIR and that Fe_2P phase formation is enhanced and modified by irradiation in EBR-II.

It is thought that the temperature range of stability and the temperature dependence of composition of the radiation induced or modified phases strongly reflects the temperature dependence of the segregation of Si and Ni. For example the decline in the nucleation rate of γ′ and the decrease in the Ni content of Laves and η phases as the neutron irradiation temperature increases above ∿525°C probably reflects a peak in the Ni segregation rate at 450–500°C. Radiation induced segregation is also thought to be a dominant factor in determining the relative proportions of phases in a given irradiation environment. For example the G and MC phases coexist during EBR-II neutron irradiation at temperatures above 550°C. However, at lower temperatures the G phase dominates to the exclusion of TiC. It is probable that the rapid segregation of Ni and Si to loops creates favorable conditions for G phase nucleation; the Ti required for MC nucleation is absorbed in the G phase and there is insufficient supersaturation of Ti for MC nucleation. On the other hand, during irradiation in HFIR conditions for the rapid segregation of Ni and Si are not as favorable; G phase formation is severely restricted and MC precipitation occurs over the entire range 300 to 650°C. Compared with irradiation in EBR-II γ′ precipitation is also restricted which is another indication that Ni and Si segregate less strongly in this environment. This is possibly related to the additional sinks in the system resulting from the nucleation of a high number density of small helium bubbles.

The effects of damage rate on phase stability in 316 and 316 + Ti alloys were discussed in earlier papers (14, 44). Subsequent work has confirmed previous observations that, during 4 MeV Ni ion irradiation at $\sim 10^{-2}$ dpa/s, very little precipitation occurs in AISI 316 over the range 525–700°C. The γ′, Laves, and σ phases do not develop; only small isolated particles of η phases are observed. In our earlier work, the major high temperature phase in neutron irradiated AISI 316 was described as a Ni- and Si-rich $M_{23}C_6$. On the basis of the more thorough diffraction and chemical analyses described in the preceding section, this phase is more correctly designated as η phase.

In the 316 + Ti alloy, both G and eta phase precipitate during Ni ion irradiation. The experimental evidence indicates that the temperature for maximum rate of formation of G phase is shifted upwards by approximately 200°C. This agrees well with the upward shift in peak swelling temperature

in AISI 316 which accompanies an increase in damage rate of $\sim 10^3$ (44). Although Laves is a major phase in 316 + Ti during both neutron irradiation and thermal aging, it does not develop during Ni ion irradiation. This is not a kinetic problem related to the brief duration of Ni ion irradiations, since Laves phase produced during prior neutron irradiation dissolved during subsequent Ni ion irradiation at approximately the same temperature. During Ni ion irradiation conditions are highly favorable for rapid segregation of Ni and Si and precipitation of G phase. The resulting changes in matrix composition are apparently sufficient to destabilize the Laves phase and induce its dissolution. The dominant influence of radiation induced segregation and G phase formation also restricts the precipitation of MC which is thermally stable at the ion irradiation temperature. The post-irradiation annealing experiment described for Ni ion irradiated 316 + Ti clearly demonstrates a reversal in the balance between these two phases on removal of the radiation induced solute fluxes.

Conclusions

1. Based upon electron diffraction and EDS analyses, nine different phases have been identified which develop in AISI 316 and 316 + Ti alloys during exposure to thermal and radiation environments. In addition, three other phases have been identified which develop during alloy melting or fabrication.

2. Determination of the temperature ranges of formation and the chemical compositions of the phases indicates that the principal effects of irradiation are to (a) induce the formation of unexpected phases, (b) enhance the kinetics of phase formation, and (c) modify the compositions of the phases formed during thermal aging.

3. The dominant factor involved in the formation of radiation-induced and radiation-modified phases is the point defect flow-induced segregation of Ni and Si to internal sinks.

4. Two of the observed phases (γ' and G) are radiation induced. The compositions of the Laves and Fe_2P phases are modified under irradiation to include Ni and Si respectively. The compositions of the phases η, $M_{23}C_6$ and MC are not significantly changed by irradiation.

5. Although radiation-enhancement of the rate of formation of certain phases is frequently observed, it is also possible for the development of thermally stable phases to be curtailed when irradiation conditions favor the development of phases driven by the segregation of Ni and Si.

References

1. E. H. Lee and A. F. Rowcliffe, Microstructural Science, 7 (1979) p. 403.

2. C.K.H. DuBose and J. O. Stiegler, Review Sci. Instruments, 38 (5) (1967), p. 294.

3. N. J. Zaluzec, "Introduction to Analytical Electron Microscopy," Ed. by John J. Hren, Joseph I. Goldstein, and David C. Joy, Plenum Publ. Corp. (1979) p. 121.

4. H. R. Brager and F. A. Garner, "Swelling as a Consequence of γ' and $M_{23}(CSi)_6$ Formation in Neutron Irradiated 316 Stainless Steel", HEDL SA 1261, (1977).

5. C. Cawthorne and C. Brown, "The Occurrence of an Ordered FCC Phase in Neutron Irradiated M316 Stainless Steel", J. Nucl. Mat. 66 (1977) p. 201-202.

6. D. G. Mazey, D. R. Harries, and J. A. Hudson, "The Effects of Si and Ti on Void Swelling and Phase Stability in 12Cr-15Ni Austenitic Alloys Irradiated with 46 MeV Ni Ions", J. Nucl. Mat., 89 (1980) p. 155.

7. F. X. Spiegel, D. Bardos, and P. A. Beck, "Ternary G and L Silicides and Germanides of Transition Elements", Trans. Met. Soc., AIME 227. (1963) p. 575.

8. G. M. Silcock, "Rates of Nitriding and Nitride Composition in Austenitic Steels Containing Titanium", Metal Science, Dec. 1978 p. 561.

9. L. E. Thomas, "Phase Instabilities and Swelling Behavior in Fuel Cladding Allcys", Trans. A.N.S. (1978) p. 151.

10. A. Westgren, Jernkont Ann. 177 (1933).

11. H. H. Stadelmaier, "Metal Rich Metal-Metalloid Phases", Developments in the Structural Chemistry of Alloy Phases, Plenum Press Corp. (1969).

12. P. J. Maziasz, "The Formation of Diamond Cubic Eta Phase in AISI 316 Stainless Steel Exposed to Thermal Aging or Irradiation Environments," Scripta Met., 13 (1979) p. 621.

13. C. G. Bolten et al., "Properties and Microstructure of 316 Stainless Steel," Mechanical Behavior of Materials, Pergamon Press, (1979) p. 183.

14. E. H. Lee and A. F. Rowcliffe and E. A. Kenik, "Effects of Si and Ti on the Phase Stability and Swelling Behavior of AISI 316 Stainless Steel," J. Nuc. Mats., 83 (1979) p 79.

15. B. Weiss and R. Stickler, "Phase Instabilities During High Temperature Exposure of 316 Austenitic Stainless Steel," Met. Trans., 3 (1972) p. 581.

16. D. V. Edmonds and R. W. K. Honeycombe, "Precipitation Processes in Solids," Met. Soc. AIME eds. K. C. Russell and H. I. Aaronson, p. 21.

17. J. I. Bramman et al., "Void Swelling and Microstructural Changes in Fuel Pin Cladding and Unstressed Specimens Irradiated in DFR," Int. Conf. on Radiation Effects in Breeder Reactor Structural Materials, Scottsdale, Ari. (1977).

18. T. M. Williams et al., "A Ni and Si Rich Phase in Irradiated FV548 Steel," J. Nuc. Mats., 82 (1979) p. 199.

19. F. Laves and H. Witte, Metallwirtschaft, Vol 14, (1935), p. 645; Vol. 15, (1936), p. 840.

20. F. Laves, "Theory of Alloy Phases" ASM Symposium, Cleveland, OH (1958), p. 224.

21. K. Andrews and P. E. Brookes, "Metal Treatment and Drop Forging," July 1951 p. 301.

22. G. S. Kasper, "The Ordering of Atoms in the Chi Phase of the Ion-Chromium-Molybdenum System," Acta Meta., 2 (1954) p. 456.

23. E. O. Hall and S. H. Algie, "The Sigma Phase", Metallurgical Reviews, 11 (1966) p. 11.

24. J. M. Silcock and A. W. Denhan, "Precipitation of NaCl-Type Carbides in Austenite and Their Behavior in Neighborhood of Grain Boundaries," Mechanisms of Phase Transformations in Crystalline Solids, Institute of Metals Monograph and Report Series, No. 33 (1969) p. 57.

30. P. J. Maziasz and R. W. Carpenter, "MC Precipitate Characterization in Austenitic Stainless Steel," 38th Ann. Proc. Electron Microscopy Soc. Amer., San Francisco, Ca, 1980, p. 384.

31. Stig Rundqvist, "Binary Transition Metal Phosphides," Arkiv För Kemi, 20 (7) (1962) p. 67.

32. J. Bentley and J. M. Leitnaker, "Stable Phases in Aged Type 321 Stainless Steel," The Metal Science of Stainless Steels, Met. Soc. AIME, (1978) E. W. Cotlings and H. W. King.

33. A. F. Rowcliffe and R. B. Nicholson, "Quenching Defects and Precipitation in a Phosphorus-Containing Austenitic Stainless Steel," Acta. Met. 20 (1972), p. 143.

34. R. S. Nelson, J. A. Hudson, and D. J. Mazey, "The Stability of Precipitates in an Irradiation Environment," J. Nucl. Mater., 44 (1972), p. 424.

35. H. Wiedersich, P. R. Okamoto, and N. Q. Lam, "A Theory of Radiation-Induced Segregation in Concentrated Alloys," J. Nucl. Mater., 83 (1979) p. 98.

36. A. D. Marwick, R. C. Piller, P. M. Sivell, "Mechanisms of Radiation-Induced Segregation in Dilute Nickel Alloys," J. Nucl. Mater., 83 (1979), p. 35.

37. N. Q. Lam and P. R. Okamoto, "Solute Segregation and Precipitation under Heavy-Ion Bombardment," J. Nucl. Mater. 78 (1978) p. 408.

38. L. E. Rehn, P. R. Okamoto, D. I. Potter, and H. Wiedersich, "Radiation Induced Segregation in Nickel-Silicon Alloys," Effects of Radiation on Structural Materials, ASTM STP 683 (1979), p. 184.

39. W. G. Johnston, W. G. Morris, and A. M. Turkalo, Radiation Effects in Breeder Reactor Structural Materials, eds. M. L. Bleiberg and G. W. Bennett (New York, Met. Soc. AIME), 1977, p. 421.

40. A. D. Marwick, "Segregation in Irradiated Alloys: The Inverse Kirkendall Effect and the Effect of Constitution on Void Swelling," Harwell Report AERE R 9111, 1978.

41. E. A. Kenik, Scripta Met., 10 (1976), p. 733.

42. A. D. Marwick, W.A.D. Kennedy, D. J. Hajey, and J. A. Hudson, Scripta Met., Vol. 12 (1978), p. 1015.

43. H. R. Brager and F. A. Garner, "Dependence of Void Formation on Phase Stability in Neutron-Irradiated Type 316 Stainless Steel," Effects of Radiation on Structural Materials, ASTM STP 683 (1979) p. 207.

44. A. F. Rowcliffe, E. H. Lee, and P. S. Sklad, "The Effect of Phase Instabilities on the Correlation of Nickel Ion and Neutron Irradiation Swelling Damage in SA 316 Stainless Steel," International Conference on Irradiation Behavior of Metallic Materials for Fast Reactor Core Components, Ajaccio, Corsica, 1979.